Nuclear dynamics of the H_2^- collision complex beyond the local approximation: Associative detachment and dissociative attachment to rotationally and vibrationally excited molecules

M. Čížek and J. Horáček
Department of Theoretical Physics,
Faculty of Mathematics and Physics, Charles University Prague,
V Holešovičkách 2, 180 00 Praha 8, Czech Republic

W. Domcke
Institute of Theoretical Chemistry,
Heinrich Heine University,
Universitätstrasse 1, D-40225 Düsseldorf, Germany

April 13, 2001

Abstract: An improved nonlocal resonance model for the description of the nuclear dynamics of the H_2^- collision complex is developed. The model is based on the *ab initio* electron-H_2 scattering data of Berman et al. at short internuclear distances, the *ab initio* data of Senekowitsch et al. for the bound $^2\Sigma_u^+$ state of H_2^- at intermediate distances, and exhibits the correct polarization interaction at large internuclear distances. Cross sections for associative detachment and dissociative attachment to rotationally and vibrationally excited molecules were calculated for a wide range of energies and angular momenta with full inclusion of nonlocal effects. The calculated associative-detachment rate constant at 300 K is $3.8 \times 10^{-9}\,\mathrm{cm^3 s^{-1}}$, which is significantly larger than the experimental value reported by Schmeltekopf et al. A series of narrow low-energy orbiting resonances was found in the associative-detachment cross section. Our results compare well with previous calculations of dissociative attachment cross sections within the nonlocal resonance model. The dissociative attachment cross section for vibrationally and rotationally hot H_2 (T = 1400 K) has been calculated and compared with the experimental data of Allan and Wong. It is demonstrated that the local-complex-potential approximation is an

excellent approximation for the associative detachment process, whereas it fails severely for the dissociative attachment process in H_2.

1 Introduction

The system H_2^- is the most fundamental molecular anion. It is unstable, with a very short lifetime ($\tau \sim 10^{-15}$ s). The dynamics of this complex is still not well understood. But it is important in a number of collisional processes. As examples of the most studied ones we mention dissociative attachment (DA)

$$e^- + H_2 \rightarrow H + H^-, \tag{1}$$

vibrational excitation (VE)

$$e^- + H_2(\nu_i) \rightarrow e^- + H_2(\nu_f), \tag{2}$$

associative detachment (AD)

$$H + H^- \rightarrow H_2 + e^- \tag{3}$$

and, for scattering energies higher than the electron affinity of H, also collisional detachment (CD)

$$H + H^- \rightarrow H + H + e^-. \tag{4}$$

Understanding of these processes is important for a number of practical applications. AD and DA determine the thermal equilibrium densities of H^- ions and H_2 molecules in many astrophysical plasmas. Neutral molecules produced in AD are vibrationally excited and the emission spectra of such molecules are quite different from those of molecules excited by ultraviolet pumping or shock excitation [1]. DA of electrons to molecular hydrogen is thought to be the primary source of the H^- ions produced in hydrogen plasmas. These ions may serve for the generation of neutral particle beams, the injection of ions into controlled thermonuclear devices, or for electromagnetic propulsion of space vehicles.

In the early models of the H_2^- dynamics the interaction between the nuclei was described in the local-complex-potential approximation [2]-[4], with empirically adjustable parameters and later with *ab initio* potentials [5], [6]. The importance of nonlocal effects was pointed out in [6]. Recently, the dynamics of nonlocal models has been studied [7], [8], [9], [10] for DA and VE in H_2.

In the present work we extend the nonlocal resonance theory to treat the AD reaction as well as DA to rotationally excited molecules. The existing nonlocal resonance model for the H_2^- dynamics [7], [8] is modified to account for the long-range behaviour of the H_2^- potential-energy function, which is of relevance for the AD reaction. VE, DA and AD processes can thus be treated within a single model with no adjustable parameters. To our knowledge, this is

the first calculation of AD cross sections as well as DA cross sections including rotational motion within the nonlocal resonance model. It should be mentioned that rotational effects on DA dynamics have been included in the largely equivalent effective-range model of Gauyacq [11]. Rotational motion is also routinely included in multi-channel quantum-defect treatments of dissociative recombination, see, e. g., [12].

We present only a brief outline of the theory and the computational procedures and a short account of the results here. A more detailed description of the methods and results will be given elsewhere [13].

2 Theoretical description

We use the projection-operator formalism (see [14] for a recent review) for the description of the quasi-molecule H_2^- formed during the collision process. We will mostly follow the notation of reference [14] here. We will employ the double-ket notation $|\,\rangle\rangle$ to denote kets in the combined Hilbert spaces of electronic and nuclear motion and single-ket notation $|\,\rangle$ for kets in either electronic or nuclear part of the Hilbert space. The treatment of the rotational degrees of freedom follows the work of Bieniek [15].

The projection-operator formalism takes advantage of the fact that all the processes of interest, (1)-(4), arise from resonant electron scattering. The resonance in the present case is the short-lived $^2\Sigma_u^+$ shape resonance [1] of H_2^-. The electronic wave function of this state can approximately be described by a square integrable function $|\varphi_d\,\rangle$. The electronic Hilbert space is divided into two subspaces by means of two projection operators

$$Q = |\varphi_d\,\rangle\,\langle\,\varphi_d|, \tag{5}$$

$$P = \int kdkd\Omega_k\,|\hat{\varphi}_k^{(+)}\,\rangle\,\langle\,\hat{\varphi}_k^{(+)}|\,. \tag{6}$$

The functions $|\hat{\varphi}_k^{(+)}\,\rangle$ spanning the P space are constructed as scattering wave functions of an electron with energy $\frac{1}{2}k^2$ and direction Ω_k, scattered by H_2 keeping the nuclei fixed. Given the electronic basis states $|\varphi_d\,\rangle$, $|\hat{\varphi}_k^{(+)}\,\rangle$, the Hamiltonian including nuclear motion can be written in the form

$$\begin{aligned} H = |\varphi_d\,\rangle[T_N + V_d(R)]\,\langle\,\varphi_d| + \int kdkd\Omega_k\,|\hat{\varphi}_k^{(+)}\,\rangle[T_N + V_0(R) + \tfrac{1}{2}k^2]\,\langle\,\hat{\varphi}_k^{(+)}| + \\ + \int kdkd\Omega_k\,|\varphi_d\,\rangle\,V_{dk}(R)\,\langle\,\hat{\varphi}_k^{(+)}| + \int kdkd\Omega_k\,|\hat{\varphi}_k^{(+)}\,\rangle\,V_{dk}^*\,\langle\,\varphi_d|, \end{aligned} \tag{7}$$

[1] The repulsive $^2\Sigma_g^+$ state has a very small influence on the low-energy scattering and it is not considered here.

where T_N denotes the kinetic-energy operator of the nuclei, $V_0(R)$ is the potential energy for the ground electronic state of H_2, $V_d(R) = \langle\, \varphi_d |\, H_{el}\, |\varphi_d\,\rangle$ is the discrete-state potential, and $V_{dk} = \langle\, \varphi_d |\, H_{el}\, |\hat{\varphi}_k^{(+)}\,\rangle$ is the discrete-state-continuum coupling. Note that in (7) we neglected the terms $\langle\, \varphi_d |\, T_N\, |\hat{\varphi}_k^{(+)}\,\rangle$ and $\langle\, \hat{\varphi}_k^{(+)} |\, T_N | \hat{\varphi}_{k'}^{(+)}\,\rangle$, which however should be small by construction of $|\hat{\varphi}_k^{(+)}\,\rangle$ (see [14]).

Using the form (7) of the Hamiltonian H, we can easily remove the P-space part of the wave function $|\Psi\,\rangle\rangle$ from the Schrödinger equation $H|\Psi\,\rangle\rangle = E|\Psi\,\rangle\rangle$. Thus we obtain for the projected state vector

$$|\Psi_d\,\rangle = \langle\, \varphi_d |\, \Psi\,\rangle\rangle \tag{8}$$

the equation

$$(T_N + V_d - E)|\Psi_d\,\rangle = \\ -\int k dk d\Omega_k V_{dk} (E - \tfrac{1}{2}k^2 - T_N - V_0 + i\varepsilon)^{-1} V_{dk}^* |\Psi_d\,\rangle, \tag{9}$$

where ε is the usual positive infinitesimal. We make use of the partial-wave expansion

$$\langle\, R|\Psi_d\,\rangle = \sum_{lm} Y_{lm}^*(\Omega_K) Y_{lm}(\Omega_R) i^l \psi_l(R) R^{-1} \tag{10}$$

and of the fact that only the p wave contributes to V_{dk} (see the discussion in [5]). Following Bieniek [15], we arrive at the radial Schrödinger equation for $\psi_l(R)$

$$\left(-\frac{1}{2\mu}\frac{d^2}{dR^2} + V_d(R) + \frac{l(l+1)}{2\mu R^2} + F_l \right) \psi_l(R) = E\psi_l(R), \tag{11}$$

where μ is the reduced mass of H_2 and

$$F_l \psi_l(R) = \int dR' \int k dk d\Omega_k V_{dk}(R) f_l^{(+)}(E - \tfrac{1}{2}k^2, R, R') V_{dk}^*(R) \psi_l(R'), \tag{12}$$

$$f_l^{(+)}(E, R, R') = \frac{1}{2l+1}\left[(l+1) g_{l+1}^{(+)}(E, R, R') + l g_{l-1}^{(+)}(E, R, R') \right], \tag{13}$$

$g_l^{(+)}(E, R, R')$ being the Green's function for nuclear motion in $V_0(R)$

$$g_l^{(+)}(E) = \left(E + \frac{1}{2\mu}\frac{d^2}{dR^2} - V_0(R) - \frac{l(l+1)}{2\mu R^2} + i\varepsilon \right)^{-1}. \tag{14}$$

The function $\psi_l(R)$ thus fulfills the Schrödinger equation with the potential $V_d + F_l$, which is nonlocal, energy-dependent and couples the nuclear motion of H_2^- with the nuclear motion of H_2, with the angular momenta differing by one.

For computational purposes it is more convenient to work with the integral (Lippmann-Schwinger) equation for $\psi_l(R)$

$$|\psi_l^{(+)}\rangle = |\phi_l\rangle + G_l^{(+)}(E)[V_d + F_l]|\psi_l^{(+)}\rangle, \tag{15}$$

instead of the integro-differential (Schrödinger) equation. Here $|\phi_l\rangle$ is the free wave

$$\langle R|\phi_l\rangle = Rj_l(KR) \tag{16}$$

and $G_l^{(+)}(E)$ is the free-particle Green's function

$$\langle R|G_l^{(+)}(\tfrac{1}{2\mu}K^2)|R'\rangle = -iKRR'j_l(KR_<)h_l^{(+)}(KR_>). \tag{17}$$

With K we denote the wave number of the relative motion of the nuclei; j_l, h_l are the spherical Bessel and Hankel functions respectively; $R_<$ and $R_>$ is smaller and bigger value of R and R' respectively.

The formula for the total AD cross section σ_{AD} is in accordance with [6], [15]

$$\sigma_{AD} = \sum_{l=0}^{\infty} \sigma_l, \tag{18}$$

where

$$\sigma_l = \frac{4\pi^2}{E} w_l \left\{ (l+1) \sum_\nu |\langle \psi_l^{(+)}|V_{dk}|\chi_{l+1}^\nu\rangle|^2 + l \sum_\nu |\langle \psi_l^{(+)}|V_{dk}|\chi_{l-1}^\nu\rangle|^2 \right\}. \tag{19}$$

The kets $|\chi_l^\nu\rangle$ denote bound-state wave functions of H_2 (ν denotes vibrational quantum number) with the bound-state energy E_l^ν. The wave number k in (19) refers to the outgoing electron. In the matrix element $\langle \psi_{l\pm1}^{(+)}|V_{dk}|\chi_l^\nu\rangle$, k is given by the energy-conservation law $\frac{1}{2}k^2 = E - E_l^\nu$. The factor w_l accounts for the nuclear spin statistics; it equals $\frac{1}{4}$ for odd l and $\frac{3}{4}$ for even l. Note that the normalization of the wave function $\psi_l^{(+)}(R)$ used here is different from [6] and is defined by equation (15). Hence the formula (19) differs slightly from the corresponding expression in [6].

For astrophysical applications it is useful to know the scattering cross sections σ_l^ν for AD processes resulting in the rotationally and vibrationally excited state $|\chi_l^\nu\rangle$ of H_2 [5]

$$\sigma_l^\nu = \frac{4\pi^2}{E} w_l \left[(l+1)|\langle \psi_{l+1}^{(+)}|V_{kd}|\chi_l^\nu\rangle|^2 + l|\langle \psi_{l-1}^{(+)}|V_{kd}|\chi_l^\nu\rangle|^2 \right]. \tag{20}$$

The DA cross section for the scattering of an electron from H_2 in the state $|\chi_l^\nu\rangle$ can be obtained from this formula using the principle of detailed balance

$$\sigma_{DA} = \frac{8\pi^2\mu}{k^2(2l+1)} \left[(l+1)|\langle \psi_{l+1}^{(+)}|V_{kd}|\chi_l^\nu\rangle|^2 + l|\langle \psi_{l-1}^{(+)}|V_{kd}|\chi_l^\nu\rangle|^2 \right]. \tag{21}$$

3 Construction of the model

We constructed a new nonlocal resonance model for the description of the nuclear dynamics of the H_2^- collision complex by modifying the long-range part of the model of Mündel, Berman, Domcke [7] (this model will be further referred to as MBD) to account for the proper long-range behaviour of the H_2^- potential-energy function.

The nonlocal resonance model is specified by the three functions $V_0(R)$, $V_d(R)$ and $V_{dk}(R)$, see eq (7). In MDB these functions are given as

$$V_d(R) = D_1 \left\{ e^{-2\alpha_1(R-R_1)} - 2te^{-\alpha_1(R-R_1)} \right\} + Q, \tag{22}$$

$$V_{dk}(R) = \frac{1}{\sqrt{2\pi}} \sum_{i=1}^{3} f_i(\tfrac{1}{2}k^2) g_i(R), \tag{23}$$

where

$$f_i(E) = A_i E^{\frac{3}{4}} e^{B_i E} \qquad i = 1,2,3 \tag{24}$$

$$g_i(R) = exp(-C_i^2(R-R_0)^2) \qquad i = 1,2 \tag{25}$$

$$g_3(R) = exp(-C_3(R-R_0)). \tag{26}$$

The function $V_0(R)$ is constructed *via* a spline interpolation of the data given by Kolos and Wolniewicz [16]. The exponent $\frac{3}{4}$ in the equation (24) is determined by the threshold law of Wigner for p-wave electron-molecule scattering [14]. The values of the parameters D_1, α_1, t, A_i, B_i and C_i were chosen to reproduce previous *ab initio* fixed-nuclei electron-scattering data for internuclear distances ranging from 1 a. u. to 3 a. u. [17]. The R-dependence of the model potential functions of MDB for $R > 3$ a.u. represents therefore a somewhat arbitrary extrapolation. This was justified by the expectation of a small sensitivity of the DA cross section to the long-range part of interaction [7]. The AD cross section, on the other hand, should be rather sensitive to the long-range behaviour of the H_2^- potential. For large internuclear distances the $^2\Sigma_u^+$ state of H_2^- is (electronically) bound and the long-range behaviour of its energy is dominated by the polarization potential (Dalgarno and Kingston [18]). The potential energy of the H_2^- ion for the internuclear distances 3−20 a.u. was calculated by Senekowitsch et. al. using *ab initio* multiconfiguration-interaction methods [19].

The energy of the H_2^- bound state in the MBD model is given by

$$V_1(R) = V_d(R) + \Delta(R), \tag{27}$$

where $\Delta(R)$ is the level shift, which is completely determined by the functions $V_0(R)$ and $V_{dk}(R)$ (see [7] for the details). It is clear that by adjusting $V_d(R)$ we can make $V_1(R)$ to be consistent with the *ab initio* results for intermediate [19] and the long [18] internuclear distances. Fortunately, we can do it in such a

way that the new $V_d(R)$ joins smoothly with the original potential $V_d(R)$ from the MBD model for $R < 3$ a.u. Thus the new model is consistent also with the fixed-nuclei electron-H_2 scattering data of Berman, Mündel, Domcke [17].

The potential $V_1(R)$ for the new model together with the old $V_1(R)$ and $V_0(R)$ of MBD are shown in figure 1. The analytic form of the new discrete state potential $V_d(R)$ is (atomic units)

$$V_d(R) = \begin{cases} 1.74e^{-2.37R} - \frac{94.4e^{-22.5/R}}{((R-2.54)^2+3.11)^2} & \text{for } R \leq 10.6 \\ -0.00845Re^{-0.35R} - \frac{2.25}{R^4} - \frac{97}{R^6} & \text{for } R > 10.6 \end{cases} \tag{28}$$

The discrete-continuum coupling element $V_{dk}(R)$ of the new model is the same as in the MBD model, see eq (23).

It should be mentioned that similar combinations of short-range, intermediate-range and long-range potentials have previously been adopted within the local-complex-potential approximation by Sakimoto [20] and Launay et al. [21]. In the intermediate range ($3 < R < 20$ a. u.) the *ab initio* $^2\Sigma_u^+$ potential-energy function is considerably more attractive than the polarization potential, which is of relevance for the AD cross section (see below).

4 Computational method

Cross sections for AD and DA were calculated from eq. (18)-(21) with the wave function $|\psi_l^{(+)}\rangle$ obtained as the unique solution of eq. (15). It is convenient to rewrite this equation in the form

$$|\psi_l^{(+)}\rangle = |u_l^{(+)}\rangle + \bar{G}_l^{(+)}(E)(F_l - W_l)|\psi_l^{(+)}\rangle, \tag{29}$$

where $\bar{G}_l^{(+)}(E)$ and $|u_l^{(+)}\rangle$ are the Green's function and the scattering solution for the local potential $V_d + W_l$, with $W_l(R)$ being a suitably chosen local potential, so that $F_l - W_l$ is "small" (see [22]). The function $|u_l^{(+)}\rangle$ is easily found as properly normalized regular solution of the Schrödinger equation in the presence of the local potential $V_d(R) + W_l(R)$, and $\bar{G}_l^{(+)}(E)$ can be written in terms of the regular and irregular solutions of this equation in analogy with eq. (17).

The nonlocal operator F_l is evaluated as follows. First we write the Green's function $g_l^{(+)}(E)$ in terms of the eigenfunctions χ_l^ν of the operator $-\frac{1}{2\mu}\frac{d^2}{dR^2} + V_0(R) + \frac{l(l+1)}{2\mu R^2}$

$$g_l^{(+)}(E, R, R') = \sum_\nu \chi_l^\nu(R) \frac{1}{E - E_l^\nu + i\varepsilon} \chi_l^\nu(R'). \tag{30}$$

Substitution of this expression for $g_l^{(+)}$ and eqs. (23) for $V_{dk}(R)$ into eq. (12), (13) yields

$$F_l(E, R, R') = \sum_\nu \chi_l^\nu(R) \left(\Delta_l^\nu(E, R, R') - \frac{i}{2}\Gamma_l^\nu(E, R, R') \right) \chi_l^\nu(R'), \tag{31}$$

$$\Delta_l(E,R,R') = \sum_{ij} g_i(R) \frac{(l+1)\Delta_{ij}(E-E^\nu_{l+1}) + l\Delta_{ij}(E-E^\nu_{l-1})}{2l+1} g_j(R'), \quad (32)$$

$$\Gamma_l(E,R,R') = \sum_{ij} g_i(R) \frac{(l+1)\Gamma_{ij}(E-E^\nu_{l+1}) + l\Gamma_{ij}(E-E^\nu_{l-1})}{2l+1} g_j(R'), \quad (33)$$

where

$$\Gamma_{ij}(E) = 2\pi f_i(E) f_j(E)$$

and

$$\Delta_{ij} = P \int_0^\infty dE' \frac{\Gamma_{ij}(E)}{E-E'}.$$

where P denotes the principal value. Note that for the functions $f_i(E)$ given by eq. (24) we can express $\Delta_{ij}(E)$ analytically [7].

A very efficient method for solving scattering problems in the presence of complicated nonlocal potentials like (31)–(33), called the Schwinger-Lanczos method (SLM), has been developed recently and is described in detail elsewhere [23]. This method is based on the Schwinger variational principle [24]. The test functions are chosen as linear combinations of the Lanczos basis functions for a certain, suitably chosen operator. This basis is constructed with a recurrence scheme from the vector $|u_l^{(+)}\rangle$. The T-matrix and wave function $|\psi_l^{(+)}\rangle$ are obtained by the inversion of a tridiagonal matrix. The SLM has been successfully used for the calculation of DA and VE cross sections (for $l = 0$) in several systems [22], [25], [26].

The SLM has been employed to solve the radial integral equation (29) for a given l. The functions $|\chi_l^\nu\rangle$ in the sum (30) were obtained with a discrete-variational-representation (DVR) method using the Fourier basis on the interval $(0, 10)$. This method also provides a discretization of the continuous spectrum [22]. Converged results were obtained with 100 Fourier functions for the DVR and 40 functions $|\chi_l^\nu\rangle$ in eq. (31) for F_l. All the functions $|u_l^{(+)}\rangle$, $|\chi_l^\nu\rangle$, $|\psi_l^{(+)}\rangle$ and the Green's function $\bar{G}_l^{(+)}$ were calculated in the interval (0,10 a. u.) on a grid of typically 2000 meshpoints. For the proper normalization of the scattering solution $|u_l^{(+)}\rangle$ and for the calculation of the Green's function $\bar{G}_l^{(+)}$ the Schrödinger equation with the local potential $V_d(R) + W_l(R)$ was solved up to $R = 100$ a. u. Convergence of the partial-wave sum for the $H + H^-$ AD cross section, eq (18), for a collision energy of 1eV requires the inclusion of angular momenta up to $l_{\max} = 30$.

We would like to stress that the calculation of the AD cross section for typically hundreds of energies (to obtain the energy-dependence) is quite demanding and the computational procedures need to be very efficient. A more detailed description of the numerical techniques which were employed in these calculations will be given elsewhere [13].

5 Results and discussion

The calculated total AD cross section for $H + H^-$ and its partial-wave components are shown in figure 2 on a doubly logarithmic scale. The results of the nonlocal model (full line) are compared with the results obtained in the local approximation (dashed line). The local approximation has been constructed as described in reference [7], *i. e.* $V_1(R)$ of eq. (27) is the real part of the local approximation. It is seen that the local AD cross section is in excellent agreement with the nonlocal result. The reason of this is the following. Only the nuclear dynamics in the region of large internuclear distances R is essential for the AD process in the low-energy region, and the nonlocal effects for such values of R are weak. The only important feature of the nuclear dynamics for small R (R less then crossing point of the potentials V_1 and V_0, *i. e.* 3 a. u.) is that the probability of the $H_2^- \to H_2 + e^-$ decay is large, and this is the feature contained in both local and nonlocal models.

The local effective potential $V_1(R) + \frac{l(l+1)}{2\mu R^2}$ depicted in figure 3 is an important tool for the interpretation of the AD process. Each partial component of the AD cross section is very small for energies below the centrifugal barrier (located in the region $R > 5$ a. u. in figure 3) and increases with energy according to the threshold law $\sigma_l \sim E^{l-\frac{1}{2}}$. The cross section decreases above the centrifugal barrier, $\sigma_l \sim \frac{l+1}{E}$. Irregularities in the region E =0.02–0.2 eV and the change of slope of the total AD cross section near $E = 0.02$ eV are associated with the sudden switching of the inner repulsive barrier from $R \simeq 2$ a.u. to $R \simeq 4$ a. u. as l increases from $l = 22$ to $l = 23$.

Upon closer inspection, the AD cross section exhibits weak and narrow resonance structures. These are clearly seen in the partial wave components $l = 23$–26 in the energy region 0.01–0.03 eV in figure 2. These resonances are typical examples of orbiting resonances, which are a consequence of the particles being trapped in the region $R \simeq 4$–8 a. u. behind the centrifugal barrier. This phenomenon increases the AD probability, since the particle trapped in the resonance state has a better chance for the tunneling into the detachment region, $R < 3$ a. u. The shape (including the resonance structures) of the partial component $\sigma_l(E)$ depends essentially only on the parameter $\beta = \frac{l(l+1)}{2\mu}$ in the effective potential. The same is true for the $D^- + D$ AD, with a higher value of μ in the expression for β. This means that in the case of $D^- + D$ the distribution of the values β is more dense and there is thus a better chance to find a resonance near the maximum of $\sigma_l(E)$ for some l. Such a resonance is more clearly discernible in the total AD cross section. This is the case for the resonance in $\sigma_{32}(E)$ for $D^- + D$ collisions. A detailed view of such a resonance structure in the total $D + D^-$ AD cross section is given in Fig. 4. The width of this resonance is of the order of 1 meV. Such a structure presumably cannot be resolved in present-day collision experiments. The measurement of these structures would be a sensitive test of the long-range part of the H_2^- potential.

Resonance structures in the $H + H^-$ AD cross section have previously been discussed by Sakimoto [20] within the local-complex-potential approximation. In Sakimoto's calculation the resonances only became visible when the imaginary part of the Bardsley-Wadehra complex potential [4] was reduced by at least a factor of 10 [20]. The imaginary part of the *ab initio* complex potential [7] is smaller than the imaginary part of the Bardsley-Wadehra potential (see Fig. 1 of [7]) and therefore resonance structures are apparent in the present calculation without artificial suppression of the imaginary part.

It has been known for some time that the local approximation performs very poorly for the DA and VE processes in H_2 [7], [8], [9], [10]. Considering that AD is just the reverse process to DA, the excellent performance of the local approximation for the AD process (cf. Fig. 2) is a bit surprising. The solution of this puzzle is given in figure 5. Here the AD cross section σ_l^ν is plotted for a number of final states $|\chi_l^\nu\rangle$, for a collision energy of 0.1 eV. It is clear from this figure that only high values of l and ν contribute to the AD cross section. For these values the difference between the local and nonlocal calculations is small (at most a few per cent). In [7] and [8], on the other hand, the DA cross sections for small values of ν and $l = 0$ were calculated. For these values of ν, l the discrepancy between the nonlocal and local calculations for AD are pronounced, but the magnitude of these cross section is so small that they contribute negligibly to the total cross section. The same feature is seen in the electron spectrum in figure 5. The difference between the local and nonlocal calculations is again small, except in the region where the probability of electron emission is small. The physical reason for this behaviour is clear. For the AD into final state $|\chi_l^\nu\rangle$ with low ν, l to occur, the particles have to get deep into the decay region (the minimum of the H_2 potential $V_0(R)$ is at $R \simeq 1.4$ a. u.). The probability for this is very small and strongly dependent on the details of the nonlocal dynamics in the region $R < 3$ a. u..

The only measurement on the $H + H^-$ AD process is the reaction rate at 300° K, $1.3 \times 10^{-9}\mathrm{cm}^3\mathrm{s}^{-1}$, of Schmeltekopf et al [27], who claim reliability of a factor of two. Our calculation gives $3.8 \times 10^{-9}\mathrm{cm}^3\mathrm{s}^{-1}$, which is almost three times larger than the experimental result and the Langevin value of $1.33 \times 10^{-9}\,\mathrm{cm}^3\mathrm{s}^{-1}$. To find out the reason why our value is so large we have compared our result with previous theoretical calculations: $2.0 \times 10^{-9}\mathrm{cm}^3\mathrm{s}^{-1}$ (Browne and Dalgarno [28]), $1.89 \times 10^{-9}\mathrm{cm}^3\mathrm{s}^{-1}$ (Bieniek and Dalgarno [5]) and 2.03 and $1.49 \times 10^{-9}\mathrm{cm}^3\mathrm{s}^{-1}$ (Launay et al. [21], their potentials V_1 and V_2 respectively). The AD reaction rate at 300° K is determined essentially by the long-range part of the potential ($R > 10$ a. u.). In the case of the models of Browne and Dalgarno [28], Bieniek and Dalgarno [5] and potential V_1 of Launay et al. [21] this part of the potential is approximately given by

$$-0.03887Re^{-0.7441R} - \frac{2.25}{R^4} - \frac{97}{R^6}. \tag{34}$$

This potential gives a reaction rate close to $2 \times 10^{-9}\mathrm{cm}^3\mathrm{s}^{-1}$. Our potential

also possesses the proper polarization asymptotics $-\frac{2.25}{R^4} - \frac{97}{R^6}$, but it is much more attractive than (34) for $R < 20\,\mathrm{a.u.}$. The potential of Senekowitsch et al. [19] is ten times deeper than (34) in the relevant region, which rises the reaction rate by almost a factor of two. The potential V_2 of Launay et al. [21] is, like our potential, adjusted to the *ab initio* data of Senekowitsch et al. [19] for $3 < R < 20\,\mathrm{a.u.}$ and should yield a rate coefficient which is significantly larger than the rate coefficient for potential V_1. The thermal rate coefficient reported by Launay et al. for potential V_2 is obviously incorrect. Sakimoto [20] has reported rate constants for very low temperatures which appear to be consistent with the present results.

If the DA cross sections for $l = 0$ of the present model are compared with the results obtained with the MBD model, we find that the modification of the long-range part of the H_2^- potential function does not change the DA cross section much. Only the threshold region is affected; the peaking of the cross section at threshold is sharper. The calculated cross section for DA to H_2 in its ground state at threshold is $4.86 \times 10^{-5}\mathrm{\AA}^2$, which is three times larger than the experimental value $1.6 \times 10^{-5}\mathrm{\AA}^2$ of Schulz and Asundi [29].

As a byproduct of the AD calculations, we have extended the calculation of the DA cross section to $l > 0$ and $\nu > 0$. To compare our results with the measurement of Allan and Wong [30], we have averaged the DA cross sections over the Maxwell-Boltzmann distribution for the temperature $T = 1400\,\mathrm{K}$. The result is shown in figure 6. To normalize the experimental data, we used the absolute cross-section value of Schulz and Asundi. The experimental curve is thus normalized in such a way that the maximum value is three times less than the maximum value of our calculation. The agreement between calculation and measurement is rather poor for higher energies ($E \sim$ 3.5-4eV), which corresponds to attachment to H_2 in its ground vibrational state. The agreement is better for lower energies, i. e., for attachment to vibrationally excited states. It should be noted that the cross section for DA to the ground vibrational state is very sensitive to details of the model, because it is determined by the details of the wave function $\psi_l(R)$ in the vicinity of the equilibrium distance of H_2, where the wave function is very small due to the rapid decay of H_2^- at short internuclear distances.

6 Conclusions

We have improved the nonlocal resonance model for H_2^- proposed by Mündel, Berman and Domcke to account properly for the long-range behaviour of the H_2^- potential-energy function. The potential function of the improved model agrees with the *ab initio* data of Senekowitsch et al. at intermediate internuclear distances and exhibits the correct polarization interaction at large distances.

Using the SLM, we have performed converged quantum calculations of DA and AD cross sections for this improved nonlocal resonance model. It has been

found that the measured thermal rate coefficient for $H + H^-$ AD is incompatible with the presumably accurate $^2\Sigma_u^+$ potential-energy function of Senekowitsch et al.. The theory predicts a value which is about three times larger than the value of $1.3 \times 10^{-9}\,\mathrm{cm^3 s^{-1}}$ reported by Schmeltekopf et al. [27]. It has also been found that the AD cross section exhibits narrow orbiting resonances. These resonances appear for collision energies between 10 and 30 meV and their width is of the order of 1 meV. The location and width of the resonances depends sensitively on the long-range part of the interaction.

The local approximation gives results close to that of the fully nonlocal calculation for the total AD cross section and for the spectra of the released electron for electron energies less than 1.5 eV. The local approximation fails when the target states with small l and ν are involved, which is the case in DA. It can be concluded that it is perfectly justified to determine an empirical local H_2^- potential-energy function by fitting experimental AD data. The fitting of experimental DA data within the local-complex-potential model, on the other hand, has no physical basis.

The comparison with experimental data shows that further improvement of the model is necessary. The calculated cross section for DA to H_2 molecules in the ground vibrational state, which is very sensitive to model parameters, is too large, and the increase of the DA cross section with ν appears to be too weak. More accurate *ab initio* calculations of the short-range part of the nonlocal H_2^- potential-energy function are necessary. More extensive and more accurate measurements of cross sections for this fundamental and practically relevant collision system would be very valuable.

Acknowledgements

We would like to thank both referees for valuable comments on manuscript. This research was carried out in part during the stay of M. Č. at the Institute of Theoretical Chemistry of the Heinrich-Heine-University Düsseldorf. M. Č. would like to thank the staff of the institute for generous help and for the friendly environment. Support by the DAAD is gratefully acknowledged.

References

[1] Black J H, Porter A, Dalgarno A 1981 *Astrophys. J.* **249** 138

[2] Herzenberg A 1967 *Phys. Rev.* **160** 80

[3] Chen J C Y 1967 *Phys. Rev.* **156** 12;
Mizuno J, Chen J C Y 1969 *Phys. Rev.* **187** 167

[4] Wadehra J M, Bardsley J N 1978 *Phys. Rev. Lett.* **41** 1795;
Bardsley J N, Wadehra J M 1979 *Phys. Rev. A* **20** 1398;
Wadehra J M 1984 *Phys. Rev. A* **29** 106

[5] Bieniek R J, Dalgarno A 1979 *Asprophys. J.* **228** 635

[6] Bieniek R J 1980 *J. Phys. B* **13** 4405

[7] Mündel M, Berman M, Domcke W 1985 *Phys. Rev. A* **32** 181

[8] Gertitschke P L, Domcke W 1993 *Phys. Rev. A* **47** 1031

[9] Hickman A P 1991 *Phys. Rev. A* **43** 3495

[10] Gallup G A, Xu Y, Fabrikant I I *to be published*

[11] Gauyacq J P 1985 *J. Phys. B* **18** 1859

[12] Schneider I F, Strömholm C, Carata L, Urbain X, Larsson M, Suzor-Weiner A 1997 *J. Phys. B* **30** 2687

[13] Čížek M, Horáček J *to be published*

[14] Domcke W 1991 *Phys. Rep.* **208** 97

[15] Bieniek R J 1978 *Phys. Rev. A* **18** 392

[16] Kolos W, Wolniewicz L 1965 *J. Chem. Phys.* **43** 2429

[17] Berman M, Mündel M, Domcke W 1985 *Phys. Rev. A* **31** 641

[18] Dalgarno A, Kingston A E 1959 *Proc. Phys. Soc. London* **73** 455

[19] Senekowitsch J, Rosmus P, Domcke W, Werner H-J 1984 *Chem. Phys. Lett.* **111** 211

[20] Sakimoto K 1989 *Chem. Phys. Lett.* **164** 294

[21] Launay J M, Le Dourneuf M, Zeippen C J 1991 *Astron. Astrophys.* **252** 842

[22] Horáček J, Gemperle F, Meyer H-D 1996 *J. Chem. Phys* **104** 8433

[23] Meyer H-D, Horáček J, Cederbaum L S 1991 *Phys. Rev. A* **43** 3587

[24] Lippmann B A, Schwinger J 1950 *Phys. Rev.* **76** 469

[25] Horáček J, Domcke W 1996 *Phys. Rev. A* **53** 2262

[26] Gemperle F, Horáček J 1997 *Czech. J. Phys.* **47** 305

[27] Schmeltekopf A L, Fehsenfeld F C, Ferguson E E 1967 *Astrophys. J.* **148** L155

[28] Browne J C, Dalgarno A 1969 *J. Phys. B* **2** 885

[29] Schulz G J, Asundi R K 1967 *Phys. Rev.* **158** 25

[30] Allan M, Wong S F 1987 *Phys. Rev. Lett.* **41** 1791

Figure 1: Potential function $V_0(R)$ of H_2 in its ground electronic state (full line) and potential function $V_1(R)$ of the $^2\Sigma_u^+$ state of H_2^- in the MBD model (dotted line) and in the new model (dashed line). *Ab initio* data of Senekowitsch et al. for H_2^- are plotted as full circles.

Figure 2: The total $H + H^-$ associative-detachment cross section (dotted-dashed line) and its partial-wave components (full lines) $l = 30, 29, ...$ (from the right). Results of the local approximation are given by dashed lines.

Figure 3: Effective potential $V_1(R) + \frac{l(l+1)}{2\mu R^2}$ for $l = 0, 10, 15, 20, 21, 22, 23, 24$ (from bottom to top). The vertical line at $R = 3$ gives the position where the potential $V_1(R)$ crosses the potential $V_0(R)$.

Figure 4: Detailed view of a resonance in the total cross section for the associative detachment of D^- in the collision with D. The partial wave $l = 32$ is responsible for this resonance.

Figure 5: Final-state distribution in $H + H^-$ associative detachment at 0.1 eV collision energy. Relative probabilities for the different final states of H_2 and the energy spectrum of the released electron are shown. The energy of the emitted electron is plotted on the x-axis, the angular momentum l of the final H_2 state on the y-axis, and the cross section σ_l^ν (arb. units) on the z-axis. The calculated electron spectrum of the nonlocal model is given by the full curve; the dotted line gives the electron spectrum obtained in the local approximation.

Figure 6: Cross section for dissociative attachment to H_2 in thermal equilibrium at 1400 K (long dashes). The full line was obtained by convolution with a Gaussian of the width 50 meV. Short dashes represent the experimental result of Allan and Wong, normalized to the threshold value of Schulz and Asundi.

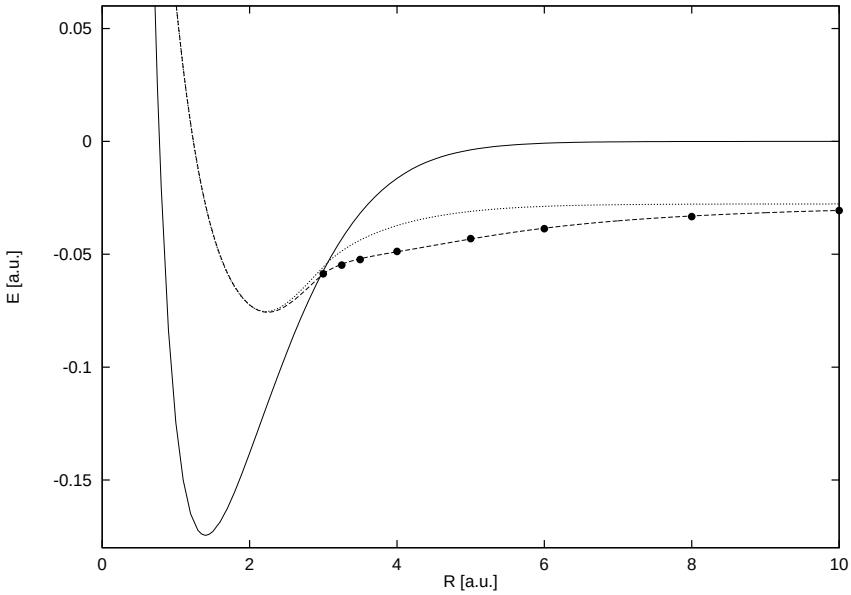

Figure 1

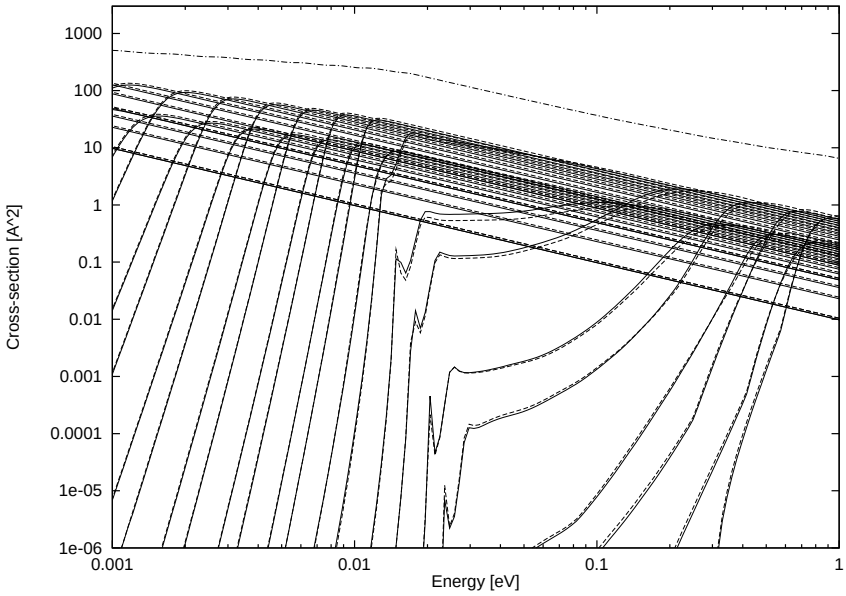

Figure 2

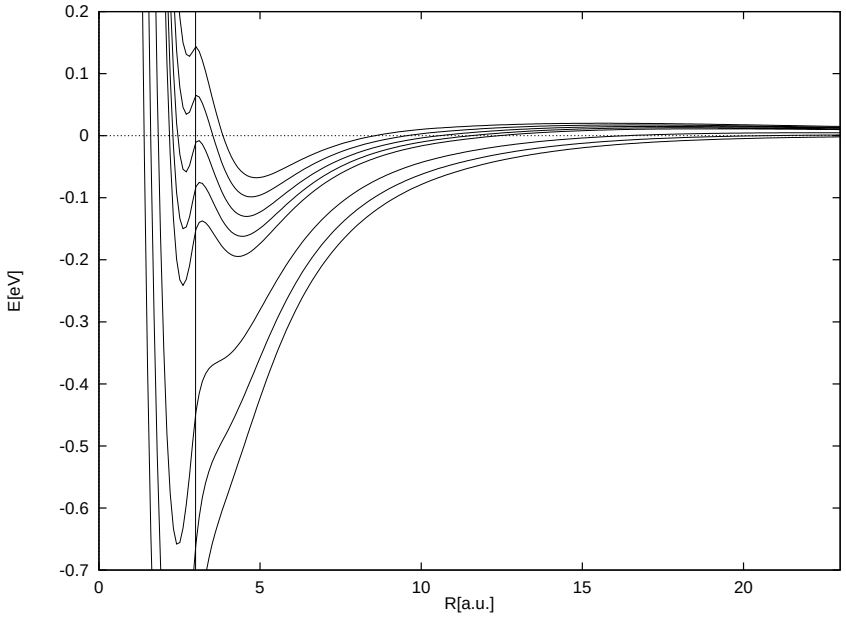

Figure 3

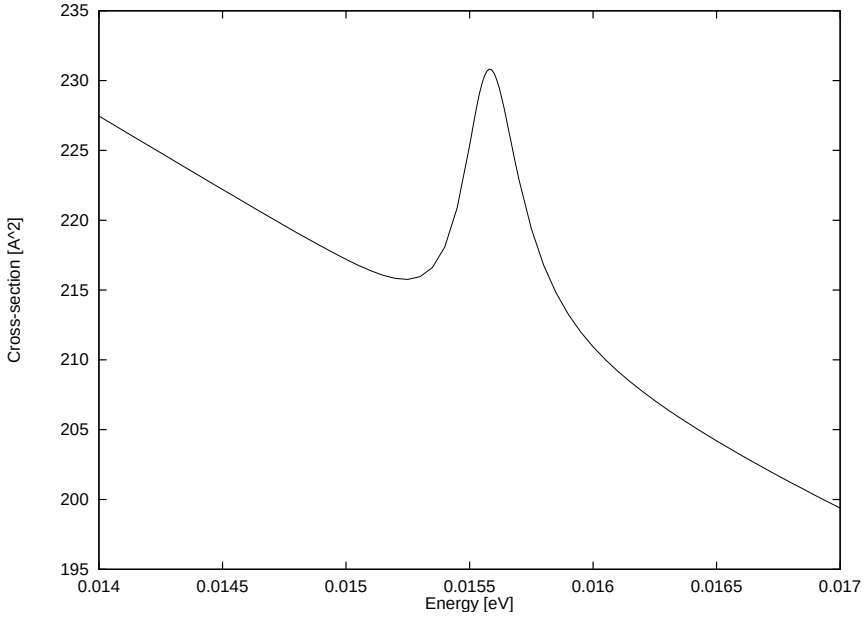

Figure 4

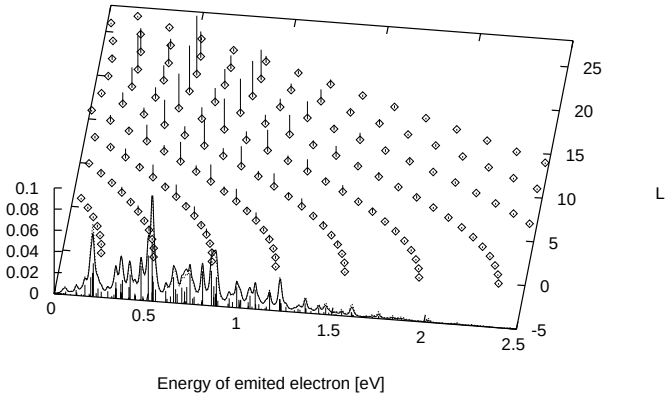

Figure 5

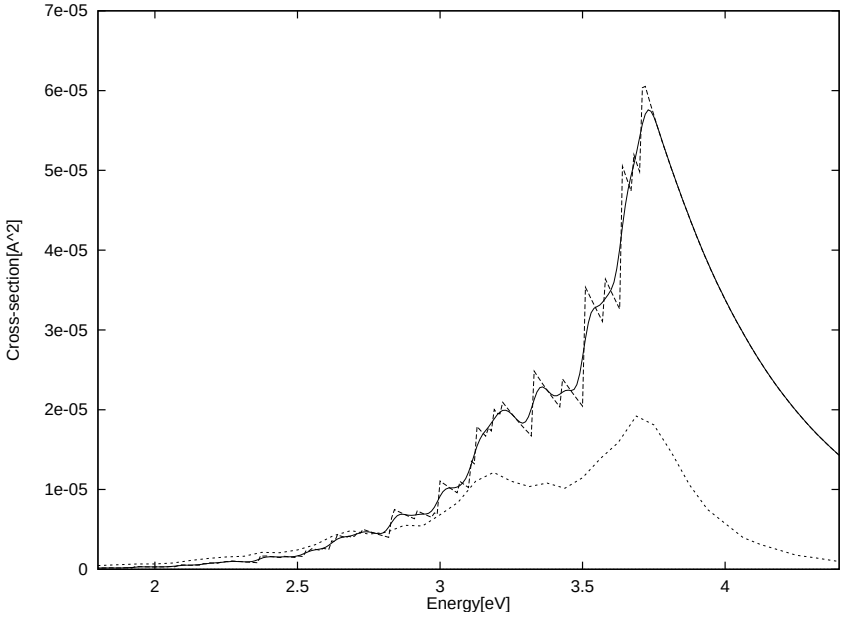

Figure 6